AD-A057 790 SOUTHWEST RESEARCH INST SAN ANTONIO TEX F/G 11/2
COMPRESSIVE STRENGTH AND INDENTATION DAMAGE IN CERAMIC MATERIAL--ETC(U)
MAY 78 J LANKFORD, D L DAVIDSON N00014-75-C-0668
UNCLASSIFIED NL

| OF |
AD
A057790

END
DATE
FILMED
10-78
DDC

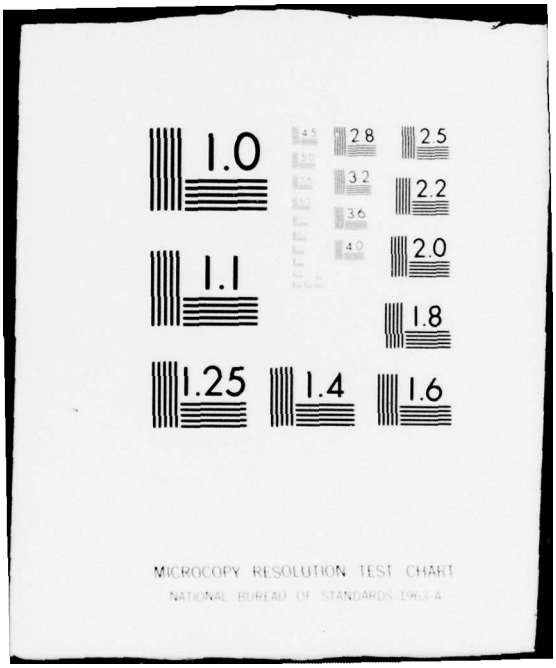
1.0
1.1
1.25
1.4
1.6
1.8
2.0
2.2
2.5
2.8
3.2
3.6
4.0
MICROCOPY RESOLUTION TEST CHART
NATIONAL BUREAU OF STANDARDS 1963-A

COMPRESSIVE STRENGTH AND INDENTATION DAMAGE IN CERAMIC MATERIALS

by
James Lankford, Jr.
David L. Davidson

TECHNICAL REPORT

ONR Contract No. N00014-75-C-0668
ONR Contract Authority NR 032-553/1-3-75(471)
SwRI Project No. 02-4231

for
Office of Naval Research
Arlington, VA 22217

by
Southwest Research Institute
San Antonio, Texas

May 31, 1978

SOUTHWEST RESEARCH INSTITUTE
SAN ANTONIO CORPUS CHRISTI HOUSTON

Unclassified

SECURITY CLASSIFICATION OF THIS PAGE *(When Data Entered)*

REPORT DOCUMENTATION PAGE

READ INSTRUCTIONS BEFORE COMPLETING FORM

1. REPORT NUMBER (6)	2. GOVT ACCESSION NO.
3. RECIPIENT'S CATALOG NUMBER (9)	
4. TITLE *(and Subtitle)* Compressive Strength and Indentation Damage in Ceramic Materials.	5. TYPE OF REPORT & PERIOD COVERED Technical Report. 1 Sept 1977 - 31 May 1978
	6. PERFORMING ORG. REPORT NUMBER
7. AUTHOR(s) (10) James/Lankford, Jr. David L./Davidson	8. CONTRACT OR GRANT NUMBER(s) (15) N00014-75-C-0668
9. PERFORMING ORGANIZATION NAME AND ADDRESS Southwest Research Institute P.O. Drawer 28510 San Antonio, Texas 78284	10. PROGRAM ELEMENT, PROJECT, TASK AREA & WORK UNIT NUMBERS NR 032-553/1-3-75 (471)
11. CONTROLLING OFFICE NAME AND ADDRESS (11) Office of Naval Research 800 North Quincy Arlington, Virginia 22217	12. REPORT DATE 31 May 1978
	13. NUMBER OF PAGES 30
14. MONITORING AGENCY NAME & ADDRESS *(if different from Controlling Office)* (12) 34p.	15. SECURITY CLASS. *(of this report)* Unclassified
	15a. DECLASSIFICATION/DOWNGRADING SCHEDULE

16. DISTRIBUTION STATEMENT *(of this Report)*

DISTRIBUTION STATEMENT A
Approved for public release;
Distribution Unlimited

17. DISTRIBUTION STATEMENT *(of the abstract entered in Block 20, if different from Report)*

18. SUPPLEMENTARY NOTES

19. KEY WORDS *(Continue on reverse side if necessary and identify by block number)*

Microplasticity	Temperature Effects	Fractography
Indentation	Acoustic Emission	Electron Channeling
Twinning	Cracking Threshold	Plastic Zone
Compressions	Microcrack Initiation	

20. ABSTRACT *(Continue on reverse side if necessary and identify by block number)*

The extent of the plastically deformed region associated with indentation in silicon carbide is determined by means of selected area electron channeling. It is found that the extent of the plastic zone beneath an indent is quite large, i.e., equal to about five times the impression radius. Microcrack formation is studied in the SEM, and the combined results are discussed in terms of current elastic-plastic indentation fracture models. The first cracks to form are radial microcracks; their morphology, and the observed

(over)

DD FORM 1 JAN 73 1473 EDITION OF 1 NOV 65 IS OBSOLETE

UNCLASSIFIED

SECURITY CLASSIFICATION OF THIS PAGE *(When Data Entered)*

328 200 LB

indentation plastic zone dimensions, support the elastic-plastic model of Perrott for indentation cracking in α-SiC.

In addition, scanning electron microscopy and acoustic emission have been used to characterize the microfracture mechanisms responsible for the temperature-sensitive compressive strength behavior of polycrystalline Al_2O_3 and α-SiC. It is determined that the early stages of damage can be related to the presence or absence of microplasticity, depending upon the ceramic. Further, local plastic flow in α-SiC is clearly observed to commence during compression at temperatures as low as 500°C, and at stresses not much greater than the tensile strength. At low temperature, hence by implication high strain rates, strain relieving plastic flow is inhibited, so that flaws of potential importance in subsequent tensile applications are introduced at compressive stresses nearly an order of magnitude lower than the compressive strength. Microvoids basic to the sintered microstructure are primary crack nuclei.

FOREWORD

This report describes the results of an experimental program oriented toward correlating compressive strength and microfracture mechanisms with indentation resistance and indentation fracture mechanisms for strong ceramics. Some of the progress made toward this goal is summarized in the following two technical papers (preprints) comprising the report.

TABLE OF CONTENTS

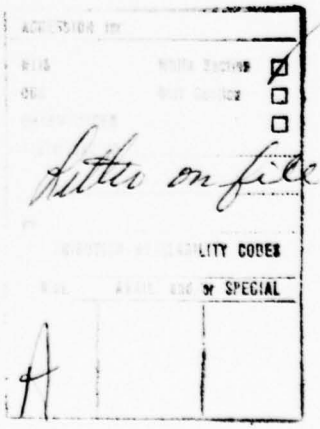

Indentation Plasticity and Microfracture in Silicon Carbide

James Lankford
David L. Davidson

Southwest Research Institute
San Antonio, Texas, USA

The extent of the plastically deformed region associated with indentation in silicon carbide is determined by means of selected area electron channeling. It is found that the extent of the plastic zone beneath an indent is quite large, i.e., equal to about five times the impression radius. Microcrack formation is studied in the SEM, and the combined results are discussed in terms of current elastic-plastic indentation fracture models. The first cracks to form are radial microcracks; their morphology, and the observed indentation plastic zone dimensions, support the elastic-plastic model of Perrott for indentation cracking in α-SiC.

1. Introduction

Strong ceramics are utilized in situations in which they often are subject to wear or erosion. Many such service applications involve elastic-plastic indentation, i.e., indent (particle) radii are sufficiently small that some irreversible deformation is associated with the indentation process. The resulting subsurface plastic zone is involved in the "damage" of a specimen through its influence upon either microcrack initiation, or subsequent crack growth.

The specific role of indentation plasticity can be inferred from consideration of current theoretical treatments of the microfracture attending indentation in brittle materials. For example, the recent Lawn-Evans model [1] for crack initiation during elastic/plastic indentation is based upon the idea of the plastic zone "seeking out" and engulfing pre-existing subsurface crack nucleation centers, so that the plastic zone size becomes critical. Similarly, Perrott [2] has examined the possibility of near-surface radial cracking, and has developed a model whose correctness depends in large measure upon the physical realism of the analytical calculation of the static and residual plastic zone boundary. Finally, Evans and Wilshaw [3] have considered indentation crack propagation using fracture mechanics and dimensional analysis concepts. In this particular case [2], the associated elastic analysis of indentation stresses for uniformly distributed contact pressure predicts that the first cracks to form should be median vents, and that the profile of the fractures should be a crescent surrounding the plastic zone and intercepting the surface. The results of the present study will be examined and interpreted from the viewpoints of these theories.

Several approaches, including X-ray diffraction, dislocation etch pitting, transmission electron microscopy (TEM), and selected area electron channeling, have been used to study damage zones in metals and ceramics. Of particular relevance to the present study are the TEM studies by Hockey, et al [4-6], of indentation damage in ceramics, and the electron channeling characterization, by Ruff [7,8], of sliding contact plastic zones in metals. In the former work, simple indentation techniques and particle impact at moderate velocity were used to produce indentation and microfracture in hard ceramics such as Al_2O_3 and SiC. The damage sites were sectioned for TEM study and the

nature of the plastic deformation determined; to a lesser extent, some idea of the spacial extent of the damage zone, especially near the surface, was obtained. On the other hand, Ruff used electron channeling to characterize the extent of the plastic zones, and the strain distributions within them, for pure metals such as copper and iron subject to sliding contact. Here there was the advantage of working with bulk samples, so that the boundary of the subsurface damage zone relative to the sliding contact could be accurately mapped. In the present case, the electron channeling approach is applied to the study of quasi-static indentation in SiC, with the principal goal of determining the extent of plastic deformation beneath a sharp indenter. A second objective is to relate observed indentation microfracture patterns to the plastic zone.

2. Experimental procedure

A silicon carbide single crystal* (α-SiC, 4H polymorph(Appendix)) approximately 7mm in cross-section x 1mm thick, having the C-axis perpendicular to the large pair of faces, was used in the study. Diamond pyramid hardness indentations were introduced into the as-grown surface using a standard microhardness tester; the indenter was applied quasi-statically, the specimen remaining under load for a total of 18 seconds.

The reason for choosing a single crystal was two-fold. First, it was desired to eliminate crystallographic effects caused by varying grain orientation. Second, the electron channeling approach requires a relatively flat, initially low dislocation density, reference surface for mapping out plastic zones. Both goals were achieved by applying indentations, at a variety of loads, in a straight line across the specimen, with their spacing adjusted so that the tips of adjoining radial cracks almost touched. The specimen was then broken in 3-point bending, producing a fracture surface passing through the center of each indent. Since the bulk of the surface was created by fast fracture, it was anticipated that this region should afford an excellent reference (minimal deformation) state, based on the TEM study of Hockey and Lawn [5], in which no dislocations were observed at the tips of arrested cracks in SiC. Orientation of the fracture surface was determined using an electron channeling pattern map, as discussed in the Appendix.

The extent of plasticity beneath the indentations was determined using the same approach the writers previously have applied to the study of fatigue crack tips in metal alloys, as described extensively elsewhere [9-11]. Briefly, numerous locations beneath, and adjacent to, an indentation are interrogated with the electron beam. Rather than rastering back and forth to produce the normal image, however, the beam is rocked through an angle of (in this study) ~7°, producing a selected area electron channeling pattern. For the electron optical system and conditions used, an area approximately 10μm in diameter was interrogated by the beam. Line acuity in the electron channeling pattern is reduced by dislocation introduced as the result of plastic deformation. The locus about the indent along which fine structure and higher order lines in the channeling patterns are observed to just begin to disappear is taken to be the plastic zone boundary (in metals, this locus corresponds to approximately 0.2% tensile strain, based on tensile calibration specimens).

*Materials Research Corporation, Orangeburg, N.Y.

3. Results

Two basic types of indentation microfracture patterns were revealed by the cleavage technique, the most common being typified by Figure 1, where several lateral cracks are seen to be associated with the indent. In addition, the outline of the radial indentation crack (arrows) lying in the plane of the fracture can be seen where it joins with the main crack. Running from the indent to the edge of the crack outline is a ledge (L), implying that the radial crack actually was made up of two segments, which grew until they met at the ledge. No median crack is visible normal to the plane of the fracture; this observation characterized 80% of the indentations.

In a few cases, a second situation prevailed, as shown in Figure 2. Here lateral cracks and a "ledge" can be seen as before, but in addition, there exists a branched median crack directly beneath the indent apex. It should be emphasized, however, that such cases were clearly in the minority, and that even for loads as high as 3500 gm (which produced impression diameters and surface radial crack lengths of approximately 50 μm and 220 μm, respectively), subsurface median cracks usually were not seen. When they were present, the median cracks usually ran only a short distance, on the order of the indentation depth, before branching into lateral cracks. They were generally closed tightly near the indent.

Locations at which channeling patterns were taken are shown by the dots in Figure 2, drawn to scale to indicate the approximate 10 μm interrogated area. Solid dots indicate channeling patterns degraded in quality by plastic flow, while open dots indicate undeformed ECPs. Figure 3 shows channeling patterns obtained from locations lying (a) within, (b) just outside, and (c) far from the plastic zone boundary sketched in Figure 2. It can be seen that Figures 3(b) and 3(c) are essentially identical, while the pattern obtained from within the plastic zone shows a marked deterioration in quality.

Although the patterns in Figure 3(b and c) are good, they are in fact not perfect. Comparison of these patterns with one taken from the virgin, as-grown surface of the crystal (Figure 3(d)) shows that the latter is considerably sharper and richer in detail, implying that there may have been a slight amount of plastic deformation associated with passage of the main crack front. Figure 3(d) does not, incidentally, show the sixfold symmetry one normally associates with a (0001) pole, because the surface was purposely tilted slightly away from 90° incidence with the beam so as to produce a channeling pattern more visually compatible with the others shown in Figure 3.

Results of the plasticity measurements can be summarized generally in terms of maximum plastic zone depth, R_y, indentation diameter 2a, and radial crack length 2c, as shown in Figure 4. Since the specimen is a single crystal, experimental scatter in these parameters is minimal. Inclusion of the indentation diameter in c is somewhat arbitrary, since close SEM inspection of indentations shows (Figure 5) that the radial cracks may not penetrate the interior of the indent; if they in fact do so, they are extremely tight cracks indeed.

From Figure 4, it is evident that both a and c have a linear relationship with R_y; the situation with regard to a can be expressed by

$$a = 0.18\ R_y \qquad (1)$$

Impressions were observed for loads as small as 2 gms, for which a = 0.6 μm,

corresponding to an extrapolated plastic zone depth of 3.3 μm. Since the load P is known to be proportional to a^2, it follows from Equation (1) that it also is proportional to R_y^2, as predicted by theory [2,3]. The crack dimension c requires a more complicated expression of the form

$$c = c^* + b(R_y - R^*) \qquad (2)$$

where c* is the hypothetical minimum (threshold) crack size, R* is the indentation plastic zone size at the hypothetical threshold for crack initiation, and b is a constant. Evaluation of these terms yields c* = 6 μm, R* = 34 μm, and b = 0.95. However, as it happens, the physical threshold for crack initiation can be determined to lie above that related to the point of intersections of the extrapolated a, c versus R_y plots. As will be reported in detail in a subsequent paper, scanning electron microscopy and acoustic emission show that the earliest cracks to form are radial cracks about 18 μm in length, corresponding to a critical plastic zone dimension $R_y \simeq 50$ μm. It is clear that at the time of crack initiation, the region below the indentation is essentially plastic. This is in fact true of the bulk of the material surrounding the impression, as shown in Figure 6. Here are summarized the results (shaded band) of channeling pattern measurements sampling various locations beneath the indentation, for loads between 200 and 3500 gms. The notation used is simlar to that of Perrott [2], whose calculation of the plastic zone boundary ($\rho = \rho'$) following unloading of an indentation is shown in Figure 7, with the normalized surface plastic zone radius chosen to be 4.0. For the particular theoretical case shown, i.e., $\rho'' = 4.0$, there is excellent agreement between the theoretical and experimental subsurface zone dimensions, e.g., ρ_y' = normalized depth of the plastic zone, and ρ_x' = normalized maximum surface projection of the plastic zone boundary.

4. Discussion and Implications

From the crack profiles revealed by the sectioning procedure, it appears that each radial indentation crack nucleates as two segments, touching the indent corners and intersecting the surface; at higher stresses, the two cracks join beneath the surface, producing a connecting ledge. Median cracks do not seem to be involved generally in the early stages of crack development. These findings are in general accord with the observations of Evans and Wilshaw [3], who studied crack development in a wide variety of ceramics, but they argue against the physical model of Lawn and Evans [1], which is based upon the idea of the median cracks being first to appear (this does seem to be the case [1] in glass). In another paper, however, we will present results which show that despite this apparent inconsistency with regard to the sequence of microfracture events, the Lawn and Evans analysis is quite successful in ordering a wide range of ceramics with respect to initial crack sizes and to the indentation loads required to initiate microfracture.

The physical model which clearly seems most representative of the prevailing state of affairs is that of Perrott [2]. The critical factors in establishing the applicability of the model are (1) that considerable subsurface plasticity must be evident, (2) in order for the hoop stress in the near-surface region to achieve tensile character, the surface plastic zone must be sufficiently large, i.e., $\rho'' > 1.65$, and (3) the first cracks to form should be radial (Palmqvist). All of these criteria are met.

assuming that the coincidence of the theoretical and experimental subsurface plastic zone dimensions (Figures 6 and 7) implies that the surface plastic zones are also in reasonable agreement, i.e., that $\rho'' \simeq 4.0$.* The basis for the good agreement here between theory and experiment apparently lies in the more realistic formulation of the stress analysis, whereby Perrott realized, and took into account, the role of the indentation plastic zone in controlling the magnitude of the contact pressure; this in turn led to an analytical result for indentation accommodation by displacement within the plastic zone, indicating divergence of the elastic solution towards a state of triaxial compression near the load axis, and towards a state of triaxial tension near the surface (Figure 7). For well-developed plasticity ($\rho'' > 1.65$), the tensile stresses generated across radial planes in the near surface region (Figure 7) were found to be of the order of the "yield" strength ($\simeq \frac{\text{hardness}}{3}$). On the other hand, the maximum tensile stress along the load axis occurs at the elastic-plastic boundary, and is equal to $Y(1-2\nu)/(7-2\nu) \simeq Y/13$, where Y is the "yield" strength, and ν is Poisson's ratio. This factor for silicon carbide amounts to around 500 MN/m^2, which is just barely equal to the tensile strength of the material. Since this relatively low stress level "samples" only a very small volume of material for nucleating flaws, it is not surprising that tensile cracks are generated first in the near surface region, where the local hoop stress produces a tensile field 13 times greater in magnitude than that along the load axis [2]. At higher loads, of course, there is a greater chance of generating median cracks below the plastic zone, since a larger material volume will be "sampled" by the plastic zone.

The threshold condition for crack initiation corresponds to a plastic zone depth of 50 μm, or apparently to a surface plastic zone dimension of about 35 μm ($\rho'' \simeq 4.0$). Perrott [2] has shown analytically that tensile values of the hoop stress at the surface occur at radii ρ less than $0.61\ \rho''$ adjacent to the boundary of the indentation. In the present case, this means that there exist regions extending nearly 9 μm out from the indentation corners, over most of which the local stress field is tensile, and considerably in excess of the tensile strength. From this, it is easy to see why the critical load for radial crack formation depends on the surface finish, decreasing as the quality of the surface diminishes [3].

The reduced sharpness of detail for channeling patterns obtained from the cleavage face in comparison with ones from the as-grown surface imply that some deformation was associated with passage of the main crack front. Hockey and Lawn [5], of course, reported an absence of dislocations near the tips of arrested indentation cracks in the same polymorph of SiC. However, the electron channeling phenomenon is extraordinarily sensitive to plastic damage, and there seems no other reasonable alternative to a dislocation-based explanation. It may be that the difference between the two experiments had to do with crack orientation relative to the specimen crystallography, although Hockey and Lawn examined foils from some two dozen indentations in SiC, which should have been a good statistical sampling. Nevertheless, other TEM work, on (β) SiC, does lend some support to this possibility. In this case, Clarke [12] examined areas immediately adjacent to the fracture surfaces of specimens broken in bending. It was found that in some grains, dislocations could be observed, depending on crystallography and, apparently, elastic constraint by other grains; in other grains, no dislocations were seen. Orientation of the crystal plane examined in this experiment was approximately (1230), Figure 8.

*This important point is supported by the near-surface TEM observations of Hockey, et al [6], in which ρ'' for SiC was estimated to be $\simeq 3.0$.

5. Conclusions

Indentations in α-SiC exhibit considerable plasticity, with the depth of plastic damage extending to about five indent radii below the indentation. The measured plastic zone parameters and the observed fractography are compatible with the elastic-plastic analysis of Perrott, which predicts that the first (threshold) cracks to form, under conditions of sufficient plasticity, are radial rather than median cracks. This is in fact observed. It is found also that $a \propto R_y$, and $P \propto R_y^2$, in agreement with theory. The electron channeling results indicate that the fracture surfaces formed under conditions of rapid crack growth have experienced some plastic flow; this may turn out to be a crystallography-sensitive effect.

Acknowledgement

The authors are grateful for the support of the Office of Naval Research, Contract No. N00014-75-C-0668, during the course of this work.

References

1. B. R. Lawn and A. G. Evans, J. Mater. Sci. 12 (1977) 2195.

2. C. M. Perrott, Wear 45 (1977) 293.

3. A. G. Evans and T. R. Wilshaw, Acta Met. 24 (1976) 939.

4. B. J. Hockey, J. Amer. Ceram. Soc. 54 (1971) 223.

5. B. J. Hockey and B. R. Lawn, J. Mater. Sci. 10 (1975) 1275.

6. B. J. Hockey, S. M. Weidernorn, and H. Johnson, "Erosion of Brittle Materials by Solid Particle Impact", National Bureau of Standards Report, NBSIR 77-1396, December 1977.

7. A. W. Ruff, Wear 40 (1976) 59.

8. A. W. Ruff, Wear 46 (1978) 251.

9. J. Lankford and D. L. Davidson, J. Eng. Mat. Tech. 98 (1976) 17.

10. D. L. Davidson and J. Lankford, J. Eng. Mat. Tech. 98 (1976) 24.

11. J. Lankford, D. L. Davidson, and T. S. Cook, Cyclic Stress-Strain and Plastic Deformation, ASTM STP 637, American Society for Testing and Materials, Philadephia (1977) 53.

12. D. R. Clarke, "Proceedings Electron Microscopy Society of America", ed. G. W. Bailey, Claitor's Pub. Div. (1975) 64.

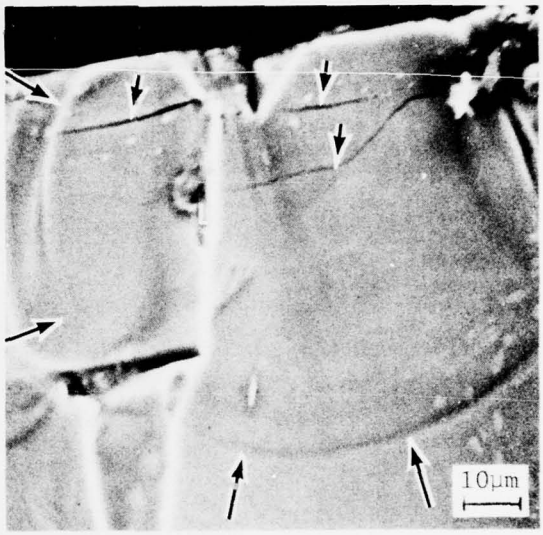

Figure 1. Section Through 3500 gm Indentation, Showing Lateral Cracks (Arrows), Ledge (L), and Outline of Radial Crack (Arrows).

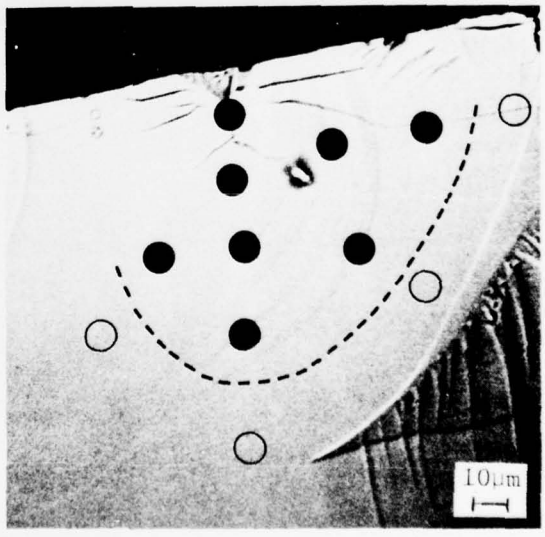

Figure 2. Section Through 1500 gm Indentation, Showing Lateral Cracks, Ledge, and Short, Branched Median Crack. Filled Circles Indicate Locations of Distorted ECP's, Open Circles Locations in Which No Damage is Seen. Dashed Line Outlines Plastic Zone Boundary.

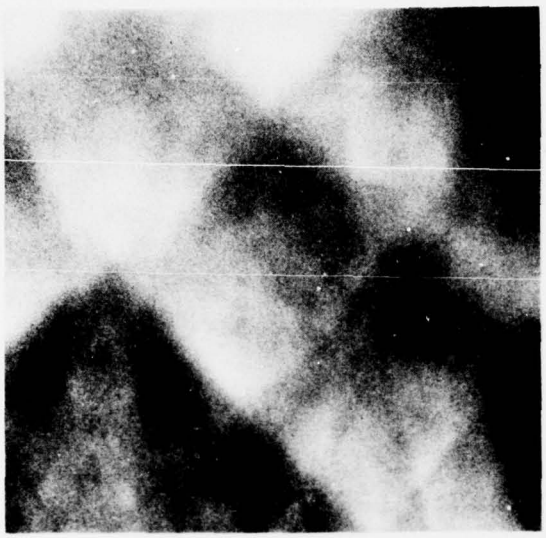

Figure 3(a). ECP Within Plastic Zone

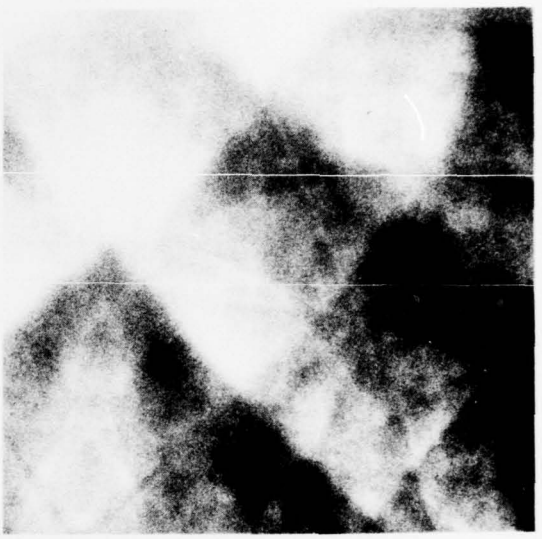

Figure 3(b). ECP Just Outside Plastic Zone

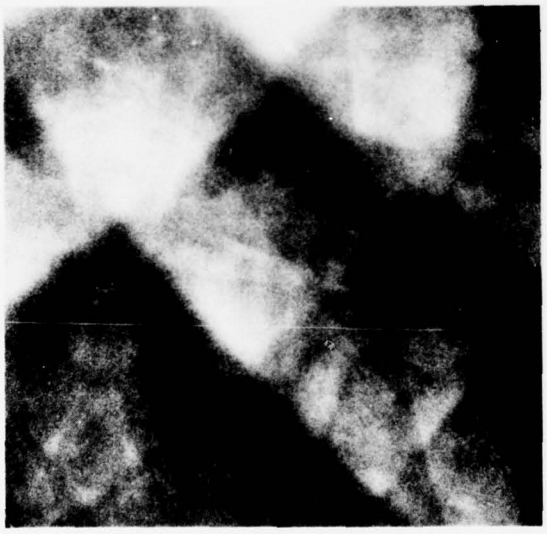

Figure 3(c). ECP Far From Plastic Zone Boundary

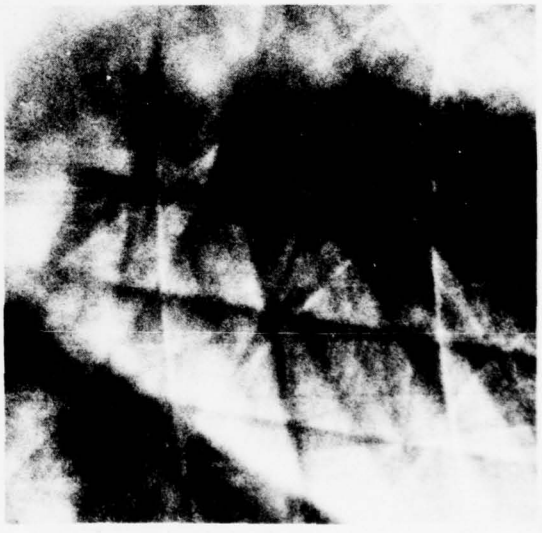

Figure 3(d). ECP From As-Grown (0001) Face

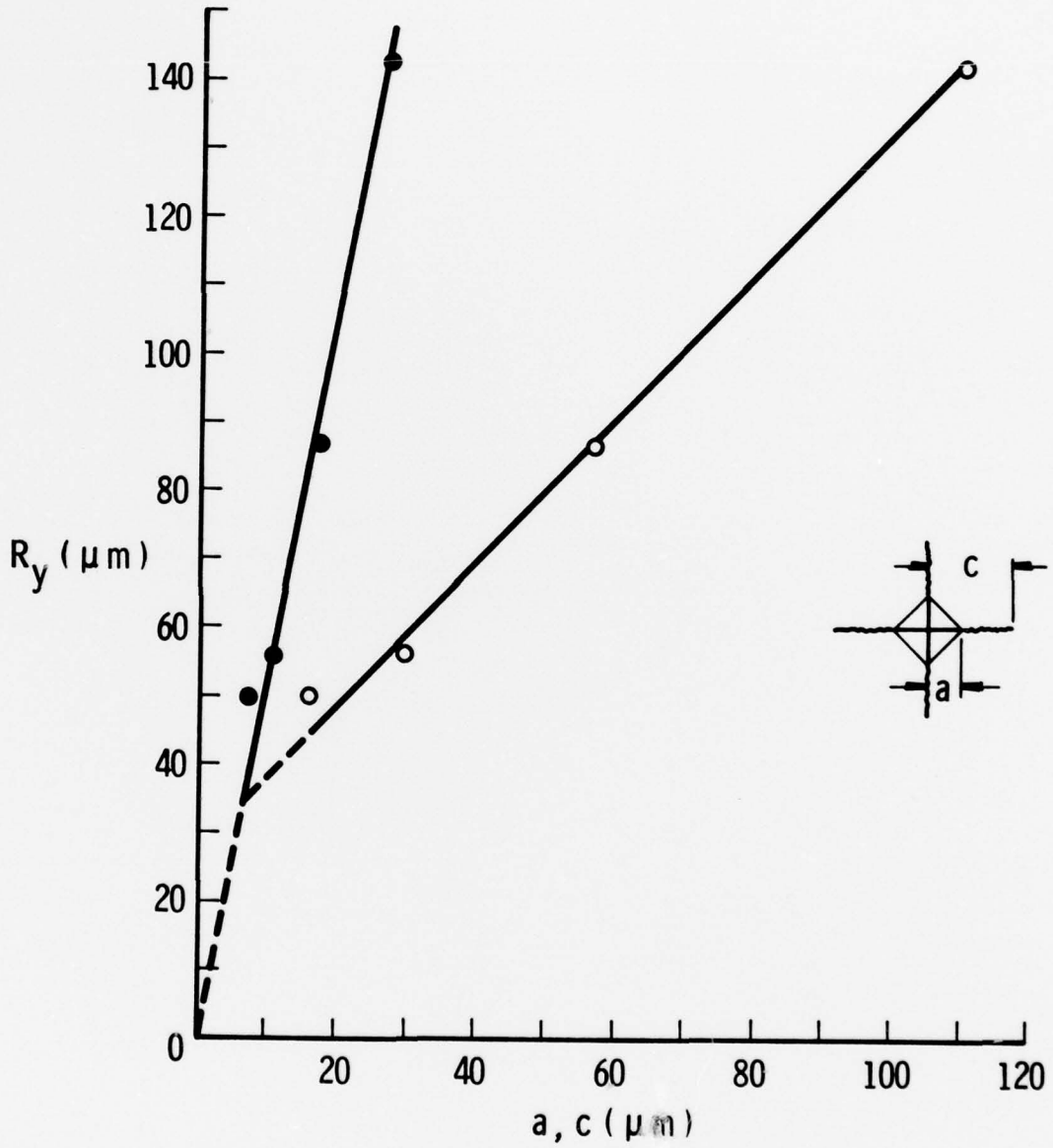

Figure 4. Plastic Zone Depth R_y Versus Impressions Radius and Crack Half-Length For α - SiC; Load Range 200-350 gm.

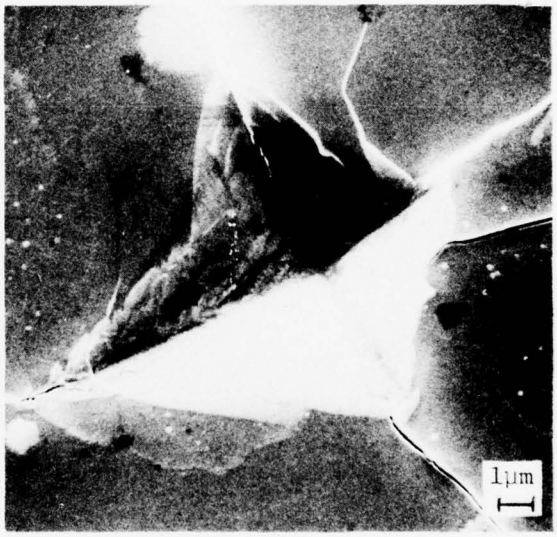

Figure 5. Indentation, 250 gm Load, Showing Closure of Radial Cracks At Edge of Indent

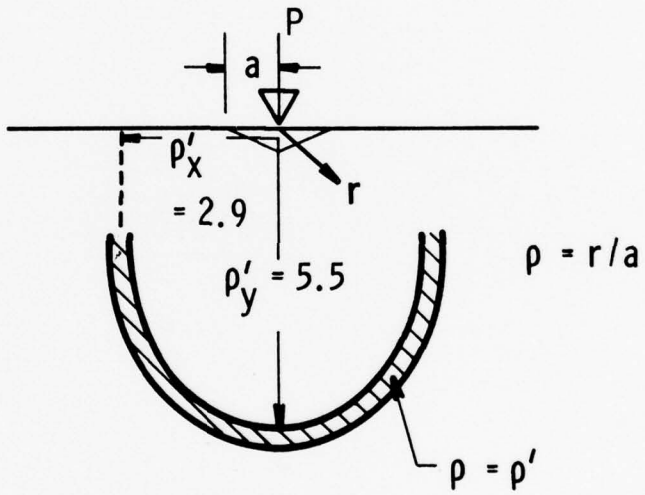

Figure 6. Experimentally Measured Subsurface Plastic Zone in α - SiC, Load Range P = 200-3500 gm

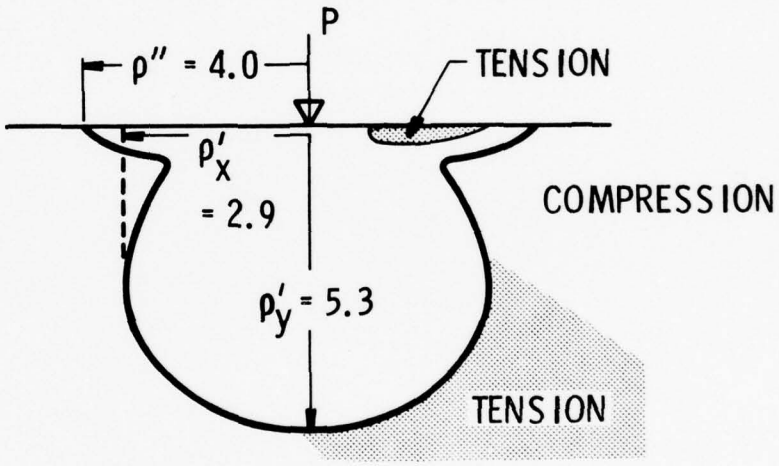

Figure 7. Calculation [7] of Plastic Zone For Elastic-Plastic Indentation Following Unloading of Indent, $\rho'' = 4.0$; Tensile Regions are Indicated by Shading Otherwise Stresses Are Compressive

Figure 8. Large Angle Electron Channeling Pattern of Fracture Surface, Showing Specimen Sides (Arrows)

Appendix

The polymorph and orientation of this material was determined using a partial channeling map, as shown in Figure A-1. This map was made from a simple crystal having (0001) planes as the largest surfaces. Tilting of the crystal away from the (0001) causes the channeling line contrast reversal seen, for example along the $(\bar{1}2\bar{1}5)$ channeling band. By working out the hexagonal interplanar angles and comparing the derived unit cell dimensions with known values[1], the polymorph may be determined.

(1) E. Parthe, "Crystal Chemistry of Tetrahedral Structures," Gordon and Breach, New York, p 107.

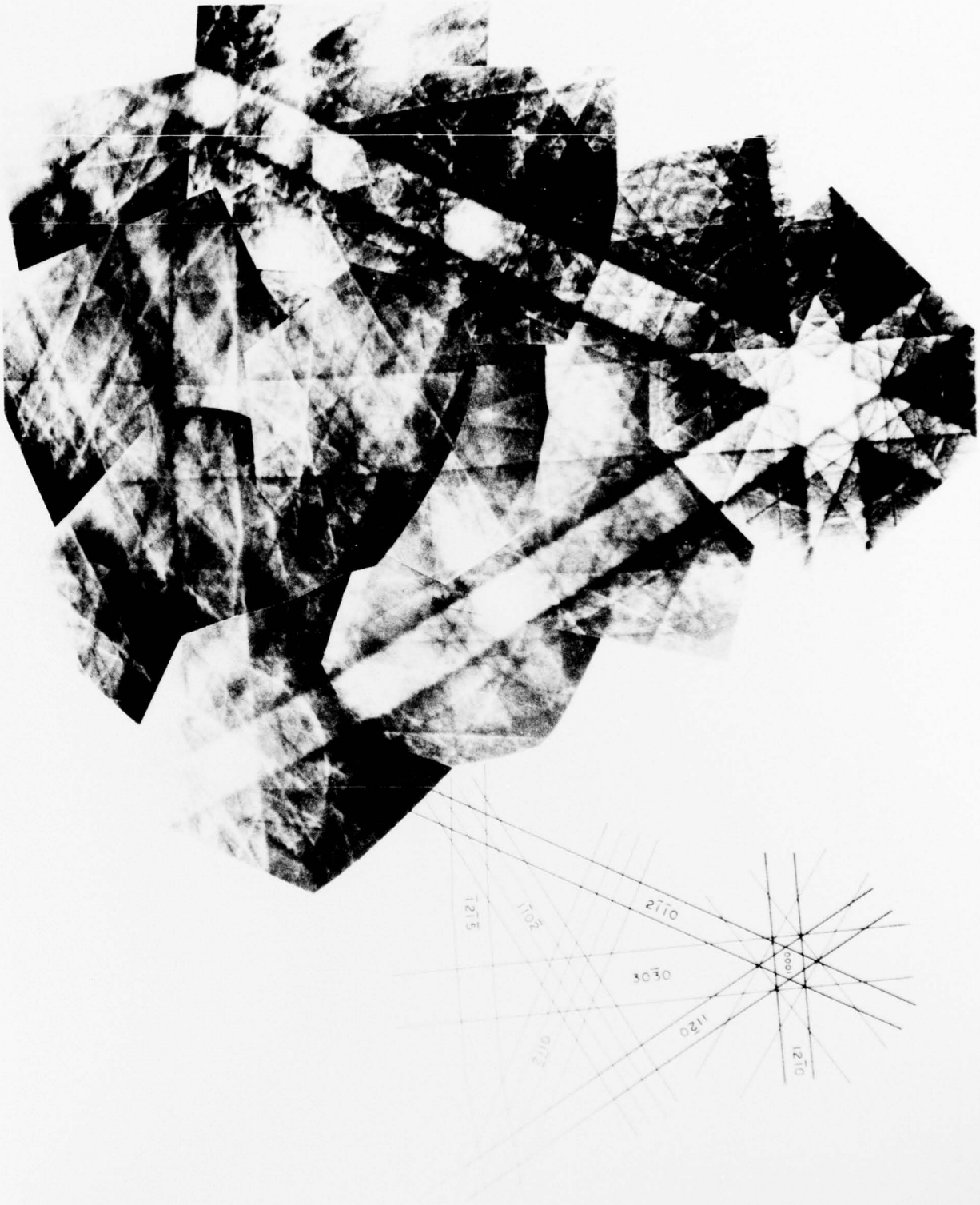

Figure A-1. Partial Electron Channeling Pattern Map, α - SiC, 30 kev

Compressive Strength and Microfracture in SiC and Al_2O_3

James Lankford

Southwest Research Institute
San Antonio, Texas 78284

Scanning electron microscopy and acoustic emission have been used to characterize the microfracture mechanisms responsible for the temperature-sensitive compressive strength behavior of polycrystalline Al_2O_3 and α-SiC. It is determined that the early stages of damage can be related to the presence or absence of microplasticity, depending upon the ceramic. Further, local plastic flow in α-SiC is clearly observed to commence during compression at temperatures as low as 500°C, and at stresses not much greater than the tensile strength. At low temperature, hence by implication high strain rates, strain relieving plastic flow is inhibited, so that flaws of potential importance in subsequent tensile applications are introduced at compressive stresses nearly an order of magnitude lower than the compressive strength. Microvoids basic to the sintered microstructure are primary crack nuclei.

I. Introduction

Compressive strength and associated damage mechanisms in strong ceramics are not as well understood as corresponding tensile factors. However, current problems involving residual compressive stress, impact, and abrasion are unavoidably concerned with compressive loadings and their effects on material behavior. Recently, the results of a study[1,2] of the temperature-strain rate dependence of compressive strength in polycrystalline alumina showed that plasticity was a key factor in initiating microfracture and controlling failure. In the present work, this earlier study is extended to higher temperatures, and α-SiC is likewise tested over a range of temperatures and strain rates. Acoustic emission and scanning electron microscopy are used to monitor and define the operative damage modes. A major objective is to compare compressive damage and strength behavior in two strong, nominally brittle ceramics.

II. Materials and Procedures

The detailed procedures followed in the compression testing have been described elsewhere, and so are presented here only briefly. Specimens of polycrystalline alumina (type GW Lucalox*) were cut from as-received rods into right circular cylinders 1.25 cm long by 0.625 cm diameter. Loading faces were ground flat within a tolerance of 1×10^{-4} cm, and then polished through 1 μm diamond. Specimens of sintered α-silicon carbide

Supported by the Office of Naval Research under Contract No. N00014-75-C-0668.

* General Electric Lamp Glass Division, Cleveland, Ohio.

were specially fabricated* to the above dimensions, and then ground and polished as above.

The Lucalox material had a grain size of approximately 25 μm, and contained a population of grain boundary and triple point voids. The ellipsoid-shaped voids were very smooth, with average maximum dimensions of about 8 μm. The SiC, on the other hand, had a grain size of only 7 μm. It likewise contained a void population, but these were much smaller, on the order of 1-2 μm in size, and sharper, than the Al_2O_3 pores. They were distributed uniformly, and did not seem to be limited to the grain boundaries.

In all of the compression tests, platens of high strength, high purity alumina† were used. As in the specimen preparation, the platen faces were ground parallel, and then polished metallurgically. Strain rates used were 7×10^{-5} sec^{-1}, 7×10^{-4} sec^{-1}, and 2×10^{-1} sec^{-1}; all tests described in this report were performed in an electrohydraulic, servocontrolled test machine, in a laboratory air environment. High temperature tests were performed in a standard resistance-type furnace adapted to the load frame. In some cases, specimens were not tested to failure, but rather were unloaded following high stress excursions, and studied in the SEM for evidence of compressive damage. Aluminum oxide specimens were palladium-coated for SEM observation, while the silicon carbide, being a semiconductor, could be examined in the uncoated state. Since the specimens of SiC were covered with a carbon-rich surface layer, it proved necessary to prepare a few specimens for observation of surface damage which had flats polished onto them (final polish was 0.25 μm diamond). These flats were examined in the SEM for compressive damage following load/unload sequences.

Acoustic emission (AE) was monitored within the frequency range 100 kHz to 1 MHz, using a PZT transducer resonant at 160 kHz (the acoustic emission setup and procedures are discussed in detail elsewhere[2]). In this study, since high temperatures were involved, the transducer was affixed to the leading ram, in order to avoid the hot zone about the specimen. Experiments indicated that the signal amplitude was not significantly altered by removal from the specimen.

III. Results

In Figures 1 and 2, the compressive test results for Al_2O_3 and SiC, respectively, are presented in terms of compressive strength (σ_c) and the threshold stress for acoustic emission (σ_{AE}), versus temperature (T). Included for comparison are graphs of tensile strength (σ_T) versus T, as determined by other workers[3,4].

The strength of alumina is fairly sensitive to strain rate, being higher for faster rates of deformation over the entire temperature range. The σ_c-T curves exhibit a perturbation at $150 \leq T \leq 400°C$ in their general decrease with temperature; this effect has been noted earlier.[2] These trends are reflected in the acoustic emission threshold stress level,

* Carborundum Company, Research and Development Division, Niagara Falls, N.Y.
† Coors AD 999, Coors Procelain Company, Galden, Colorado.

above which twinning and twin-related cracking already has been observed[2] for temperatures to 890°C. The tensile strength behaves similarly, decreasing with temperature, leveling off at 200°C, and then dropping again at higher temperatures; in this case, however, the degree of the strength differential is considerably less than for the compressive strength. It is interesting to note that at low temperature, σ_{AE} is on the order of six times σ_T.

Sintered α-SiC exhibits behavior which is strikingly different from that just described. As shown in Figure 2, the compressive strength increases monotonically with temperature up to the highest temperatures at which tests have been run.* This trend is mirrored by σ_T. However, the acoustic emission threshold stress level first increases up to room temperature, and then decreases with higher temperatures. Moreover, σ_{AE} at low temperature barely exceeds σ_T, and at 550°C, is little more than twice σ_T. It appears, from the present limited data, that σ_c is not so strain rate sensitive as is aluminum oxide.

Some idea of what is happening to cause the results shown in Figures 1 and 2 can be derived fractographically, as well as by examining the microfracture events which are visible on the specimen surfaces. Aluminum oxide, for example, displays a striking temperature-dependent transition in fracture behavior, as shown in Figure 3. At low temperature, the fracture surface is primarily transgranular; as the temperature increases, fracture becomes increasingly intergranular, until around 1200°C, where failure is almost totally via intergranular separation. This general trend also has been observed[3] for tensile failure, but there the effect does not seem to be so dramatic.

Surface observations of microfracture in the Al_2O_3 have been previously described[1,2] for temperatures up to 890°C, so only the newer results for temperatures in excess of that range will be presented here. As shown in Figure 4, twinning (T) and possibly slip are present at T = 1260°C. The fine deformation bands seemed to have no influence upon crack initiation. The twins, however, did sometimes initiated cracking by forming cracks at the twin/parent interface (Figure 4(a)); once these cracks encountered grain boundaries, they changed mode to intergranular, rather than nucleating further transgranular cracks in adjacent grains as had been the case at lower temperature. Often, the twins which formed had no apparent effect on crack nucleation. Instead, as shown in Figure 4(b), local cracking ensued at grain boundaries (either at triple points or possibly subsurface intergranular voids), and remained intergranular as the crack grew.

Very little difference could be seen in the SiC fracture surfaces over the temperature range studied, i.e., up to 500°C, fracture is transgranular (Figure 5). Many voids can be seen, and often they are located near the center of fracture facets, possibly having served as microfracture nuclei.

The surfaces of unfailed specimens loaded to 3500 $MNm^{-3/2}$ at room temperature and 500°C were studied for evidence of microfracture. At 23°C, numerous short, axially-oriented, void-initiated cracks were

---

* Tests at higher temperature cause problems because of softening of the Al_2O_3 platens, necessitating the fabrication (in progress) of SiC specimens having reduced gage sections so as to lower the stresses on the platen surfaces.

seen, with most of these appearing to be transgranular. At 500°C, extensive evidence of plastic deformation was found (Figures 6 and 7), generally nucleated at sharp-cornered intrinsic voids. The slip bands usually stopped when they encountered a grain boundary (Figure 6(a)) or another void. Cracks which formed did not seem to be as directly related to this plasticity as did those reported earlier in Al_2O_3, whereby twins were directly responsible for cracking. The slip bands appeared to represent instead, efforts by the material to accommodate the imposed strains. Cracks which nucleated were usually formed at voids, and again were predominantly axial transgranular in orientation. There were instances, however, in which cracks either formed in (Figure 6(a)) or adjacent to (Figure 7) slip bands.

IV. Discussion and Implications

By considering the physical basis for the acoustic emission threshold stress level, it is possible to rationalize the σ_c-T behavior of both materials, even though the SiC acoustic emission results do not mirror the corresponding strength data. In this regard, we will appeal to some of our earlier work,[1,2] in which it was suggested that the observed acoustic emission in Al_2O_3 was caused by twinning.

Above the threshold, twinning in Al_2O_3 is observed; at the same time, some cracking can be seen, always (at temperatures to 890°C) associated with twins, which serve as nuclei[1,2]. At higher temperatures, the recent results reported above show that while acoustic emission still is obtained, the stress level required decreases, as does the strength, yet many of the observed cracks, in particular intergranular ones, are no longer twin-nucleated. Moreover, some of our recent work (to be published shortly) indicates that the threshold for indentation cracking in Al_2O_3 can be delineated with acoustic emission, while sub-threshold indentation plasticity causes no emission. Further, the first stage of the acoustic emission count rate versus compressive strength plot, which had previously[2] been associated with twinning in alumina, has been found to exhibit almost identical slopes for both Al_2O_3 and SiC. Consequently, it now appears that σ_{AE} for Al_2O_3 is related to the cracking which accompanies some of the twinning observed above the threshold. The high threshold for low temperature (hence high strain rates, which are too rapid to allow AE measurement) then results from the fact that thermally activated twinning, hence twin-initiated cracking, is inhibited, thereby moving the AE stress level up. At high temperature, grain boundary microfracture ensues, constituting a change in crack mode, and reflected in σ_c and σ_{AE} decreasing at a more rapid rate above 500°C.

Twinning in SiC is not nearly so important a mode of deformation as in Al_2O_3. The following scenario is suggested to explain the observed results. At low temperatures, slip is suppressed, and unable to affect local strain relaxation as it does at higher temperatures. Consequently, axial cracks nucleate readily at the intrinsic, high stress concentration voids. As the temperature increases, so does the acoustic emission threshold stress level, since limited plastic deformation begins to relieve the requirement for cracking. At still high temperatures, plastic flow starts to contribute to the cracking process, in addition to providing some strain relief. The contribution to cracking thereupon causes the decrease in σ_{AE} noted at 500°C, while the compressive strength per se continues to rise. The latter is reasonable; while some cracks are

forming at a slightly lower threshold level, others are being prevented from forming. Since compressive failure is a crack coalescence process,[1] the net effect is to increase σ_c.

In both of these materials, the explanations of compressive strength behavior are dependent upon microplasticity concepts. This is in general accord with the empirical correlation drawn several years ago by Rice[5] between compressive strength, hardness, and plasticity for ceramic materials.

To the knowledge of the writer the observation of significant plasticity in α-SiC at 500°C is the most solid, clear-cut evidence to date for the low homologous temperature plastic flow capability of SiC under uniaxial loading. A very limited amount of data had previously been obtained for β-SiC by Clarke,[6] using TEM. His work showed the presence of limited dislocation activity within certain grains at the fracture surfaces of tensile polycrystalline specimens, with other grains being devoid of plasticity.

The fact that σ_{AE} is so low for low temperatures, hence presumably high strain rates, has implications with regard to design against failure. It appears that rapid compressive loadings which might normally be considered acceptable, in view of the high compressive strength, may cause unacceptable damage, from the point of view of the cracks introduced, and their possible role under tensile loads. From the preceding discussion concerning the nature of σ_{AE}, it seems clear that the flaws introduced above this level are cracks, not twins or dislocations, whose distribution and size should be taken into account by any fracture mechanics-based analysis of an SiC specimen (structure) subject to compression and tension.

It also is clear that the sharp-edge microvoid population inherent in the sintered α-SiC is a serious problem in terms of crack nucleation. While it may be that their absence would not greatly affect the intrinsic compressive strength, which, again, involves crack coalescence, they clearly have a profound effect in controlling the stress level at which compressive microfracture first occurs in SiC.

Finally, while SiC compressive strength per se is not very temperature sensitive over the range investigated, σ_{AE} is rather sensitive to this factor. For applications where damage (cracks) introduced by compression is a consideration, temperature may be very important in controlling the degree of damage for a given compressive stress level.

References

1. J. Lankford, "Compressive Strength and Microplasticity in Polycrystalline Alumina," J. Mater. Sci., 12, 791-796 (1977).

2. J. Lankford, Fracture Mechanics of Ceramics, Vol 3, Edited by R. C. Bradt, D. P. H. Hasselman, and F. F. Lange, Plenum, NY, 245-255 (1978).

3. O. Johari and N. M. Parikh, Fracture Mechanics of Ceramics, Vol 1, Edited by R. C. Bradt, D. P. H. Hasselman, and F. F. Lange, Plenum, NY, 399-420 (1974).

4. E. H. Kraft and J. A. Coppda, "Thermo-mechanical Properties of Sintered Alpha Silicon Carbide," presented at Fifth Army Materials Technology Conference, "Ceramics for High Performance Applications - II," Newport, Rhode Island, March, 1977.

5. R. W. Rice, Materials Science Research, Vol 5, Edited by W. W. Kriegel and H. Palmour, Plenum, New York, 195-229 (1971).

6. D. R. Clarke, Proceedings Electron Microscopy Society of America, Edited by G. W. Bailey, Claitor, Baton Rouge, 1975.

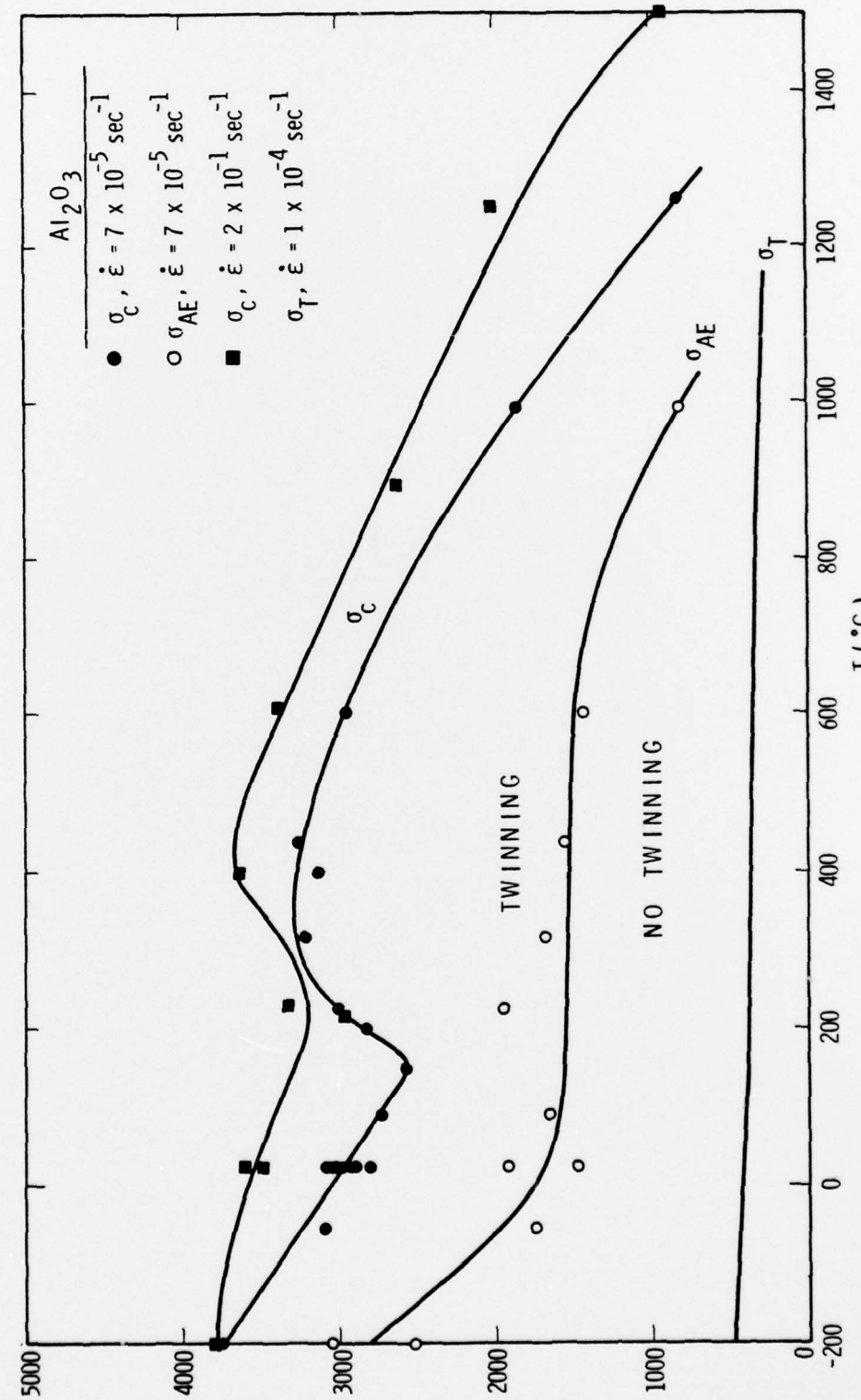

Figure 1. Compressive Strength Versus Temperature For Al_2O_3

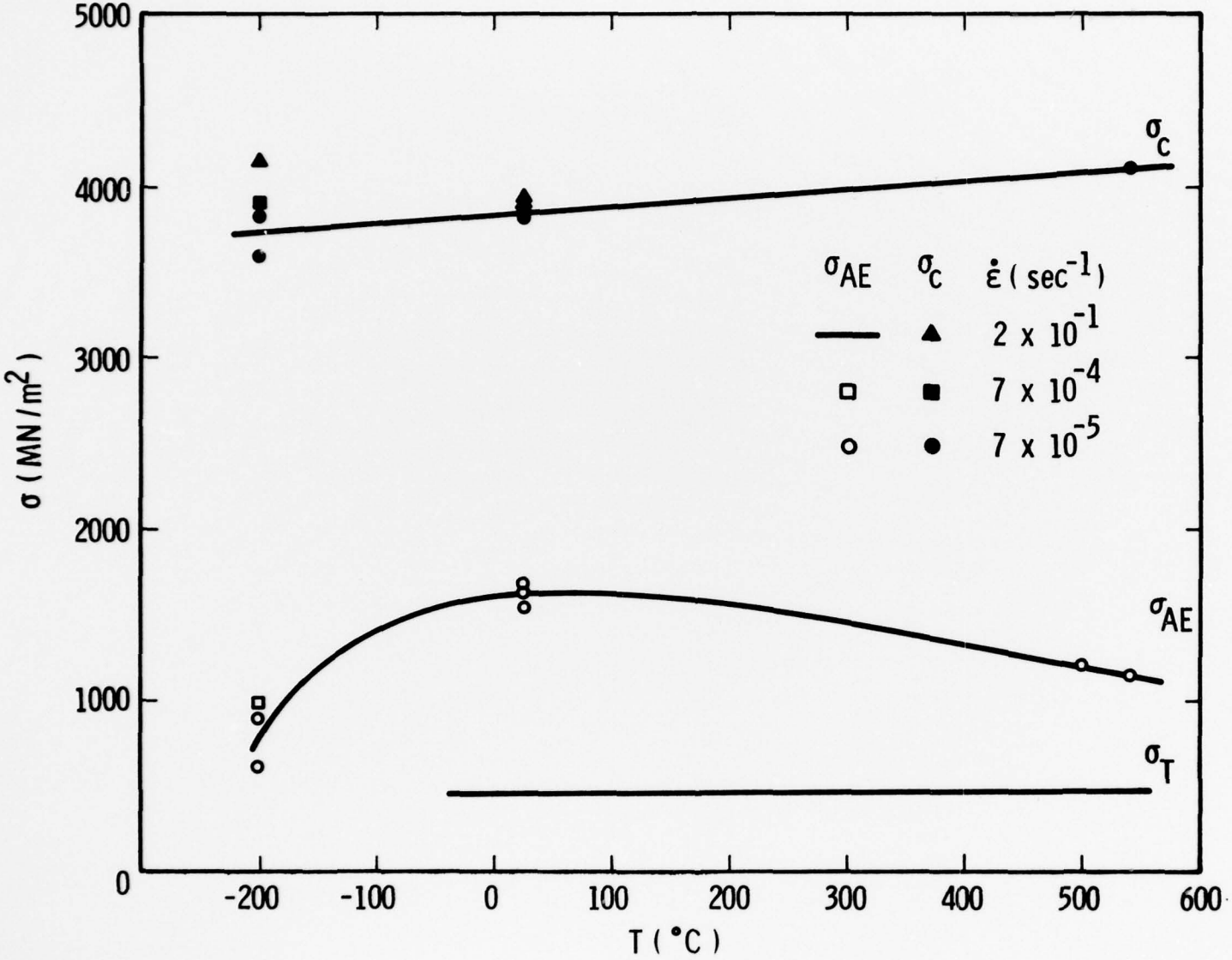

Figure 2. Compressive Strength Versus Temperature
For α-SiC

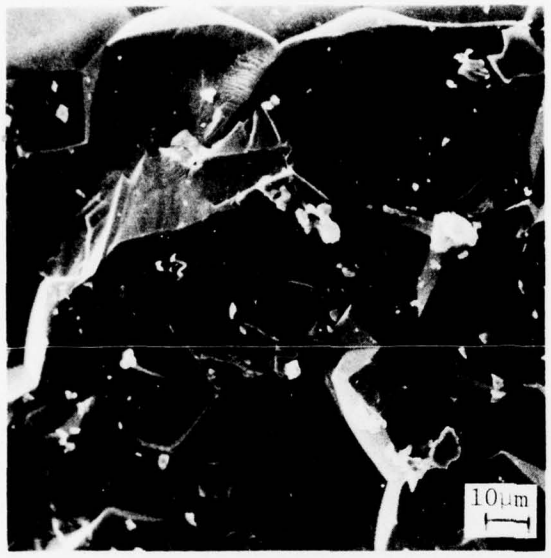

(a) T = -200°C

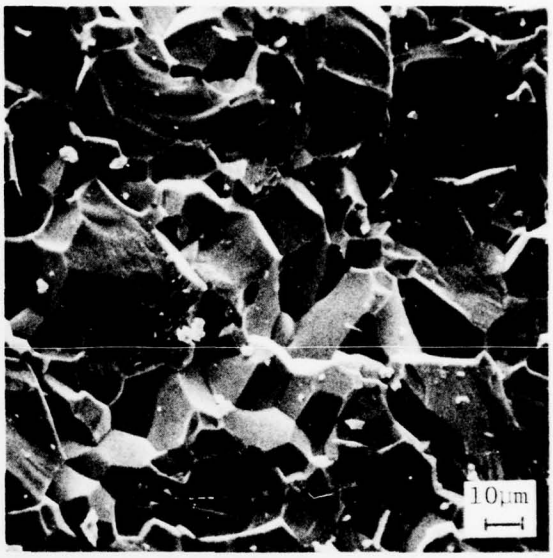

(b) T = 443°C

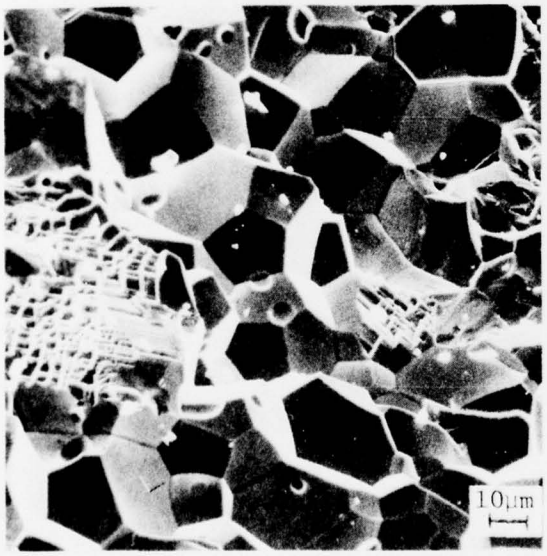

(c) T = 892°C

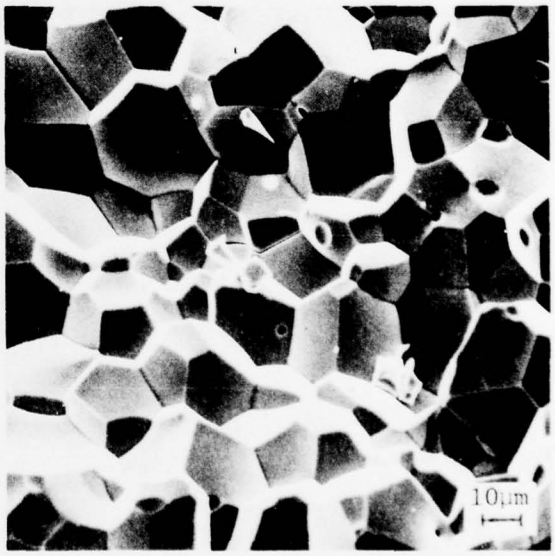

(d) T = 1260°C

Figure 3. Fracture Surfaces for Al_2O_3 Failed Under Compression, $\dot{\varepsilon} = 7 \times 10^{-5}$ sec^{-1}

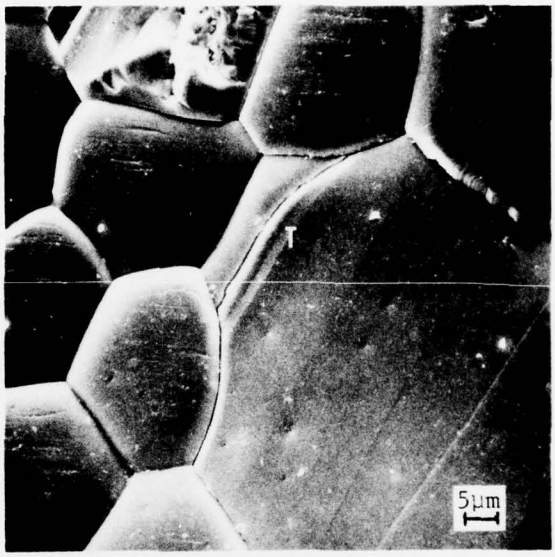

(a) *Transition from twin (T) - nucleated,* transgranular cracking to intergranular cracking (arrow) T = 1260°C

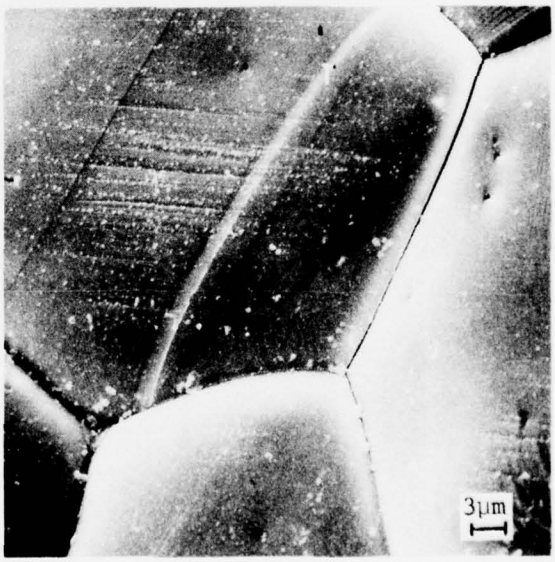

(b) Twinning (T) with no cracking; intergranular cracking (arrow) T = 1260°C

Figure 4. Crack Initiation In Al_2O_3 Under Compressive Loading At High Temperature

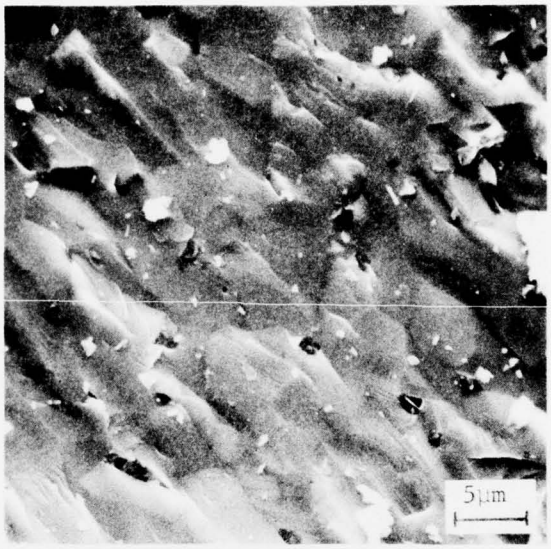

(a) T = 23°C

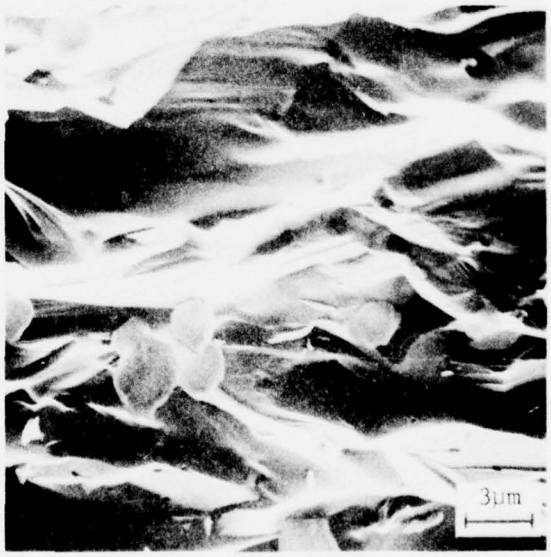

(b) T = 500°C

Figure 5. Fracture Surfaces For α-SiC Failed Under Compression, $\dot{\varepsilon} = 7 \times 10^{-5}$ sec^{-1}

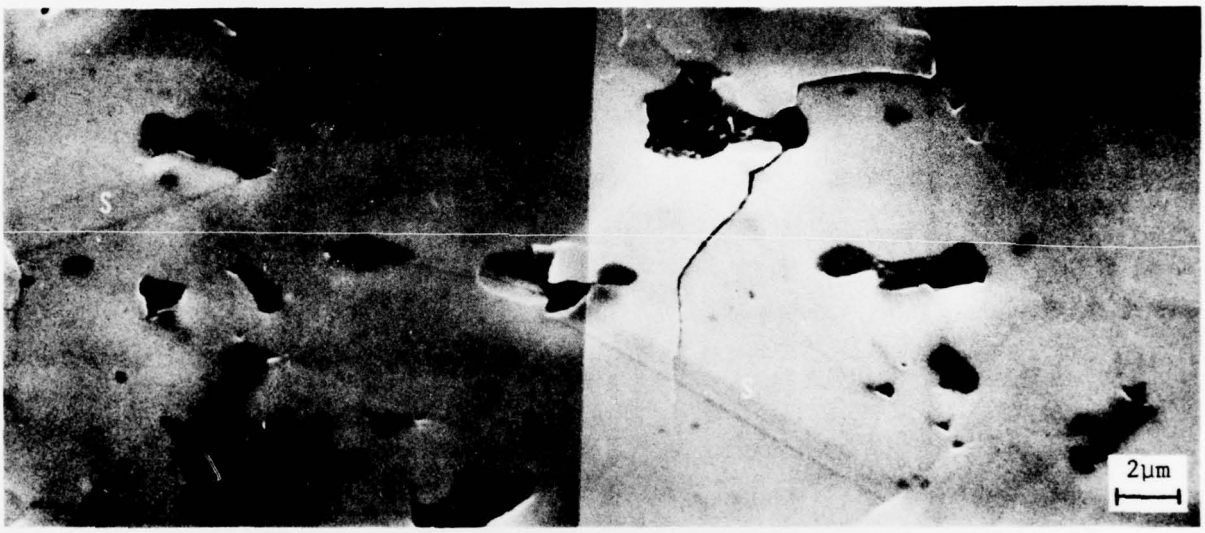

(a) Void nucleated slip (S)

(b) Slip

Figure 6. Slip(S) In α-SiC Caused By Compressive Loading, T = 500°C, $\dot{\varepsilon}$ = 7 x 10^{-5} sec^{-1}

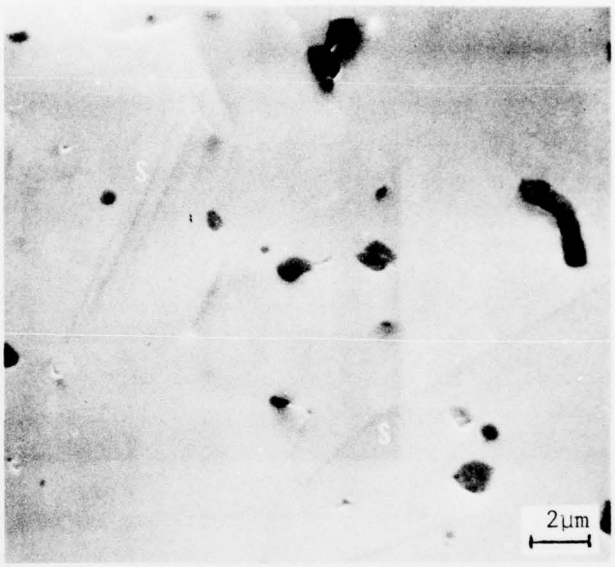

(a) Grain boundary and void-nucleated slip (S)

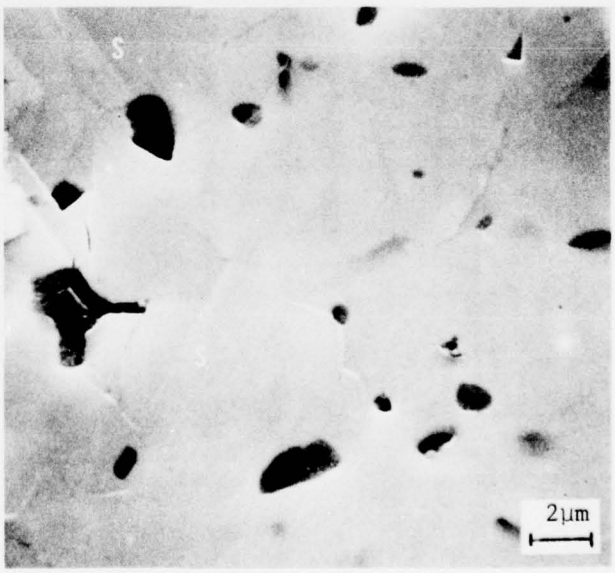

(b) Grain boundary-nucleated slip(S)

Figure 7. Slip(S) In α-SiC Caused By Compressive Loading, T = 500°C, $\dot{\varepsilon} = 7 \times 10^{-5}$ sec^{-1}